ELSEVIER

20 June 1997

Chemical Physics Letters 272 (1997) 96–102

CHEMICAL PHYSICS LETTERS

Infrared picosecond laser control of acceleration of neutral atoms: model simulations for the collision pair O + H

M.V. Korolkov [1], B. Schmidt

Institut für Physikalische und Theoretische Chemie, WE 3, Freie Universität Berlin, Takustrasse 3, D-14195 Berlin, Germany

Received 11 February 1997; in final form 21 April 1997

Abstract

The quantum dynamics of an atomic collision pair interacting with the electric field of an infrared sub-picosecond laser pulse is investigated by means of propagation of representative wavepackets. Depending on the optimal choice of the laser pulse, two competing types of scattering events are encountered. First, for continuum → bound transitions, effective (85%) vibrationally state-selective photoassociation reactions $O + H \rightarrow OH(v)$ are induced by stimulated emission [Chem. Phys. Lett. 260 (1996) 604]. Second, for non-resonant cases, laser-controlled acceleration of the colliding atoms can be achieved. Laser field optimization allows one to design the energy distribution of the scattered atoms. © 1997 Published by Elsevier Science B.V.

1. Introduction

In collision of atoms or radicals some amount of electronic charge can be transferred among the collision partners. Apart from the electrostatic attraction, this process also gives rise to a dipole moment thus opening the way to manipulation of these systems by external electric fields. Interaction of this dipole moment with an infrared laser pulse can lead to two different processes. One possible event is a continuum → bound transition leading to photoassociation $O + H \rightarrow OH$ which has been investigated recently for the first time [1]. Although the process of laser-controlled infrared photoassociation exhibits many analogies with the reversed process of photodissociation in the electronic ground state [2–5] there are fundamental differences arising from the bimolecular nature of associative collisions [1]. First of all, one has to control the timing of the laser pulse with respect to the collision event. Second, the continuum → bound transitions have to compete with continuum → continuum transitions both of which are accessible by one-photon transitions. The latter ones give rise to acceleration of the scattered particles. This process of inelastic scattering is known in the literature as collision induced absorption [6–8].

The purpose of this Letter is to demonstrate the possibility of collision induced acceleration of colliding atoms by means of ultrashort infrared (IR) laser pulses, at least for a simplified model case, which may serve as a reference for future investigations of more realistic models or experiments. Special em-

[1] Permanent address: B.I. Stepanov Institute of Physics, Belarus Academy of Sciences, Skaryna ave. 70, 220602 Minsk, Republic of Belarus.

PII S0009-2614(97)00512-5

phasis will be on the competition between elastic and inelastic scattering events and photoassociation of the collision complex leading to stable products in the electronic ground state. In this context, we will mainly be concerned with the aspect of selectivity of the competing processes with respect to the most important parameter of the process, namely the carrier frequency of the laser pulse. The main objective will be the efficiency of the process of laser induced acceleration avoiding the various first or higher-order resonance frequencies corresponding to permanent association of the collision partners. Another important parameter controlling laser induced acceleration is the intensity of the lasers used. In the present Letter, it will be discussed how the probability of elastic versus inelastic scattering can be controlled and the role of multi-photon transitions will be reflected.

2. Model

The initial state of the system is chosen to be a free scattering state of the collision pair $^{16}O(^3P) + ^1H(1s)$ similar to our previous study [1]. The relative motion of the collision partners is modeled as superposition of free waves with a Gaussian distribution of momenta leading to a localized wavepacket in the internuclear distance coordinate r

$$\psi(r,t=0) = \left(\frac{2}{\pi a^2}\right)^{1/4} \exp\left[ik_0 r - \left(\frac{r-r_0}{a}\right)^2\right]. \tag{1}$$

Here the two atoms are assumed to be initially at an average distance of $r_0 = 1.641$ nm which is well outside the interaction region. The uncertainty in the distance coordinate is $\Delta r = a/2$ with $a = 0.5212$ nm. For a relative mass of $m = 0.9482$ u the initial (relative) momentum $k_0 = -66.14$ nm^{-1} corresponds to a relative velocity of the collision of 4.43 km/s or to a center of mass collision energy of $E_0 = \hbar^2(k_0^2 + 1/a^2)/2m = 777.7$ cm^{-1} (≈ 0.1 eV) which is in the typical order of magnitude of atomic beam experiments [9,10].

As the atoms are approaching each other, they start to interact through the potential energy function $V(r)$ with each other and through the dipole moment function $\mu(r)$ with the external field. Hence, the Hamiltonian of the relative motion is given by

$$\hat{H}(r,t) = \frac{-\hbar^2}{2m}\frac{\partial^2}{\partial r^2} + V(r) - \mu(r)\mathscr{E}(t), \tag{2}$$

where $V(r)$ stands for the Morse potential function

$$V(r) = D_e\{\exp[-\beta(r-r_e)] - 1\}^2 - D_e \tag{3}$$

of the $X^2\Pi$ electronic ground state of OH. The parameters were chosen to be $D_e = 43763$ cm^{-1}, $r_e = 96.36$ pm, and $\beta = 22.47$ nm^{-1} [11]. The interaction with an external electric field $\mathscr{E}(t)$ which is assumed to be linearly polarized along the molecular axis is treated here in semiclassical electric dipole approximation where the molecular dipole moment $\mu(r)$ is modelled by a Mecke function[12]

$$\mu(r) = q r \exp(-r/r^*) \tag{4}$$

with parameters $q = 1.634|e|$ and $r^* = 60$ pm representing OH bonds in the water molecule [13]. The electric field $\mathscr{E}(t)$ of the laser is modeled by a $\sin^2$ pulse shape

$$\mathscr{E}(t) = \mathscr{E}_p \sin^2\left(\frac{\pi t}{\tau_p}\right)\cos(\omega_p t), \quad 0 \leqslant t \leqslant \tau_p \tag{5}$$

with amplitude $\mathscr{E}_p$ and carrier frequency ω_p. As in our previous work, we consider a constant pulse duration of $\tau_p = 0.5$ ps.

The time evolution of the initial state (Eq. (1)) under the influence of the Hamiltonian (Eq. (2)) is governed by the time-dependent Schrödinger equation

$$i\hbar\frac{\partial}{\partial t}\psi(r,t) = \hat{H}(r,t)\psi(r,t). \tag{6}$$

Because of difficulties of calculating matrix elements for continuum → continuum transitions in the state representation, this equation is solved numerically using a Fourier collocation scheme [14,15]. The wave function $\psi(r,t)$ is represented on an equidistant grid in coordinate space with 8192 grid points ranging from 2.6 pm up to 26.5 nm. For the propagation in time we use the split-operator technique which is an $\mathscr{O}(\Delta t^3)$ approximation in the time step Δt [16,17]. Here a time step of 0.05 fs was chosen which is equivalent to approximately 100 steps per cycle of the laser pulses specified below.

3. Results

To begin with, we will consider the probability of the two competing processes of elastic or inelastic scattering (non-reactive) versus photoassociation (reactive) as a function of the frequency ω_p of the laser pulse (Eq. (5)). In the following, we restrict ourselves to the frequency regime between 2400 and 3900 cm^{-1}. For one-photon associative events, this corresponds to continuum → bound transitions from a continuum state with $E_0 = 777.7$ cm^{-1} down to the vibrational states $v = 17$ and the $v = 16$ of the OH Morse oscillator, with eigenenergies of $E_{17} = -1884.2$ cm^{-1} and $E_{16} = -2796.3$ cm^{-1}, respectively (see Fig. 1a).

Fig. 1b shows the frequency dependence of the probability of forming an OH molecule at the end of

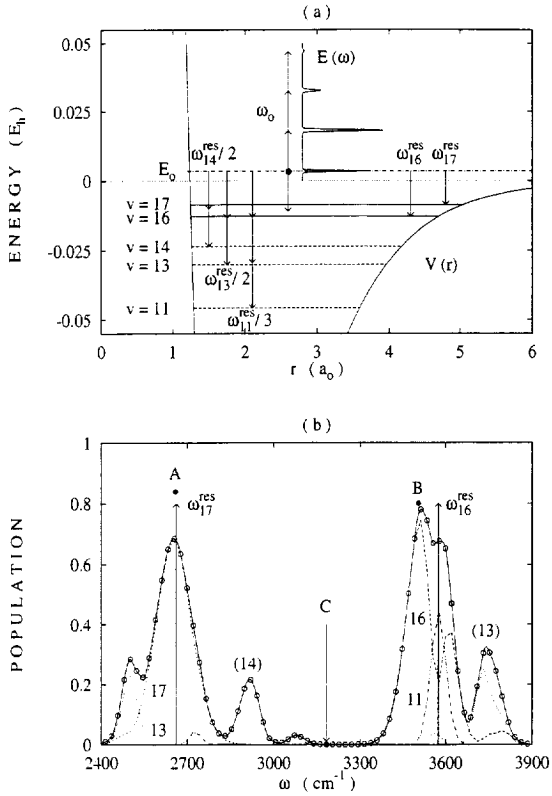

Fig. 1. (a) Potential energy curve and energy levels of the OH Morse oscillator. The dot–dashed horizontal line shows the energy of the incoming wavepacket, the solid and dashed lines indicate the bound-state levels that can be reached by one and more-photon processes in the frequency range between 2400 and 3900 cm^{-1}. The vertical arrows denote the corresponding resonance frequencies. The energy distribution of scattered particles illustrates the effect of laser acceleration for $\mathscr{E}_p = 25.71$ GV/m and $\omega_p = 3182.4$ cm^{-1}. In atomic units ($a_0 = 52.92$ pm, $E_h = 219450$ cm^{-1}). (b) Well population at the end of the laser pulse ($t = 0.5$ ps) as a function of the laser frequency ω_p for a field of $\mathscr{E}_p = 25.71$ GV/m (solid curve with open circles). The vertical arrows indicate the resonance frequencies for state-selective photoassociation $O + H \rightarrow OH(v)$ for $v = 16$ and $v = 17$. The solid points A and B indicate optimized conditions (ω_p and $\mathscr{E}_p$) for these processes while point C marks a frequency suited for laser induced acceleration (see Fig. 2).

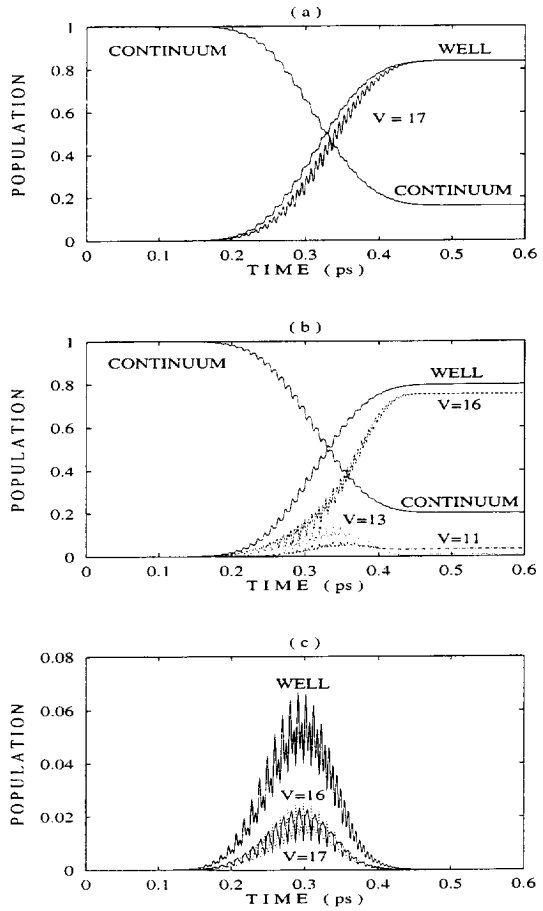

Fig. 2. Population dynamics induced by optimized laser pulses (see solid points in Fig. 1). Part (a) shows the continuum, bound states, and total well population dynamics for a laser pulse with $\mathscr{E}_p = 6.23$ GV/m and $\omega_p = 2658.9$ cm^{-1} optimized for $v = 17$ photoassociation. Part (b) shows the same but for a pulse with $\mathscr{E}_p = 8.21$ GV/m and $\omega_p = 3502.8$ cm^{-1} optimized for $v = 16$. Part (c) shows the well population for a pulse with $\mathscr{E}_p = 7.46$ GV/m and $\omega_p = 3182.4$ cm^{-1} optimized for laser induced acceleration.

the laser pulse ($t = 0.5$ ps) for a given field of $\mathscr{E}_p = 25.71$ GV/m. The solid curve clearly shows two main peaks located close to the resonance conditions for one-photon transitions (vertical arrows) for photoassociation reactions $O + H \rightarrow OH(v)$ at $\omega^{res}_{E_0 \rightarrow v=17} = 2661.9$ cm^{-1} and $\omega^{res}_{E_0 \rightarrow v=16} = 3574.0$ cm^{-1}. Additionally, there are two secondary maxima in the vicinity of the frequencies corresponding to resonant two-photon transitions at $\omega^{res}_{E_0 \rightarrow v=14}/2 = 2968.4$ cm^{-1} and $\omega^{res}_{E_0 \rightarrow v=13}/2 = 3693.8$ cm^{-1} and a third-order transition at $\omega^{res}_{E_0 \rightarrow v=13}/3 = 3609.2$ cm^{-1} (see also Fig. 1a). The contribution of the individual levels to the total well population are also shown in Fig. 1b.

First, the one-photon associations shall be investigated separately. For pulses which are optimized with respect to the well population in the $v = 17$ and $v = 16$ level (see the solid points A and B in Fig. 1b), the time-dependent population dynamics is depicted in Fig. 2a and Fig. 2b. In the former case, about 83.9% of the probability can be transferred from a continuum state into bound states of the well,

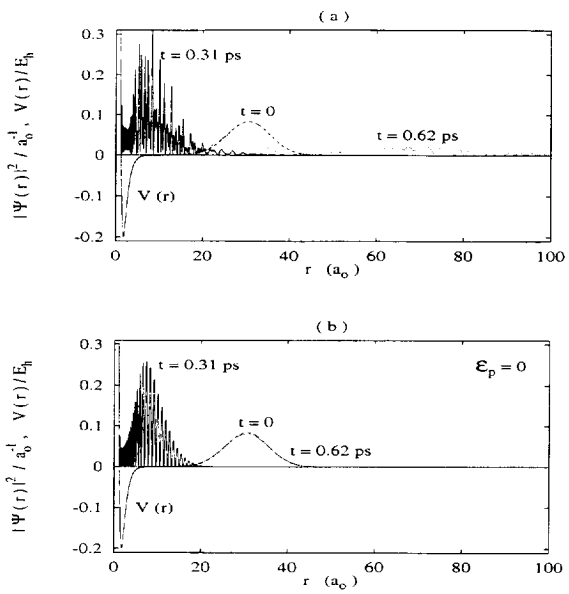

Fig. 3. Snapshots of the wavepacket dynamics for O + H collisions in position space representation (in atomic units $a_0 = 52.92$ pm) at three different instants of time: $t = 0$ (dot–dashed), $t = 0.31$ ps (solid), and $t = 0.62$ ps (dotted). Part (a) shows the laser induced acceleration process for $\mathscr{E}_p = 7.46$ GV/m and $\omega_p = 3182.4$ cm^{-1}. For comparison, purely elastic scattering ($\mathscr{E}_p = 0$) is shown in part (b).

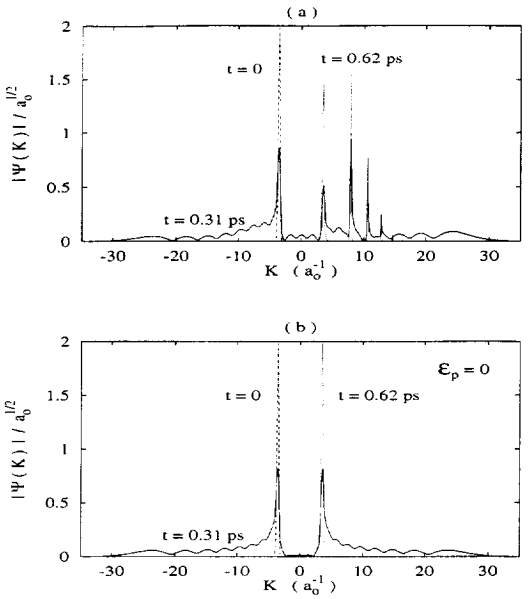

Fig. 4. Snapshots of the wavepacket dynamics for O + H collisions in momentum space representation (in atomic units $a_0^{-1} = 18.897$ nm^{-1}) at three different instants of time: $t = 0$ (dot–dashed), $t = 0.31$ ps (solid), and $t = 0.62$ ps (dotted). Part (a) shows the laser induced acceleration process for $\mathscr{E}_p = 7.46$ GV/m and $\omega_p = 3182.4$ cm^{-1}. For comparison, purely elastic scattering ($\mathscr{E}_p = 0$) is shown in part (b).

almost exclusively (> 99.9%) into the $v = 17$ state (see Fig. 1b). For the $v = 16$ state, the overall efficiency of 79.8% is similar (see Fig. 1c). However, the vibrational selectivity of the process is deteriorated considerably due to the near coincidence with the two-photon transition to the $v = 13$ level and the three-photon transition to the $v = 11$ level.

Furthermore, the optimal frequency range for elastic or inelastic scattering events is evident from Fig. 1b. In the interval between 3150 and 3350 cm^{-1} there are no resonances for continuum $\rightarrow$ bound transitions and about 100% of the probability amplitude is scattered non-reactively. This process is illustrated in Fig. 2c for $\omega_p = 3182.4$ cm^{-1} (see point C in Fig. 1b). In the time interval between 200 and 300 fs there is some population building up in the well which, however, does not exceed 7%. This population is distributed approximately equally between the $v = 16$ and $v = 17$ state. The probability of finding bound states is going down again during the next 100 fs and is almost zero at the end of the laser pulse

which indicates that no permanent association has taken place and that 100% of the wavepacket has been scattered.

This process of non-associative scattering is visualized in Fig. 3. The comparison of the position space representations of the wavefunction $|\psi(r,t)|$ in parts (a) and (b) of the figure clearly shows the effect of the laser pulse on the O + H collision pair. In the case of no external field ($\mathscr{E}_p = 0$, Fig. 3b) there is purely elastic scattering. The choice of our initial conditions for r_0 and k_0 is such that after 0.62 ps the wavepacket has returned to its initial position and shape but with reversed momentum. At intermediate times, e.g. $t = 0.31$ ps, there is an interference between ingoing and outgoing portions of the wavefunction similar to a standing wave (see Fig. 3b). This has to be contrasted to the case where a laser pulse interacts with the system. Apart from irregular-

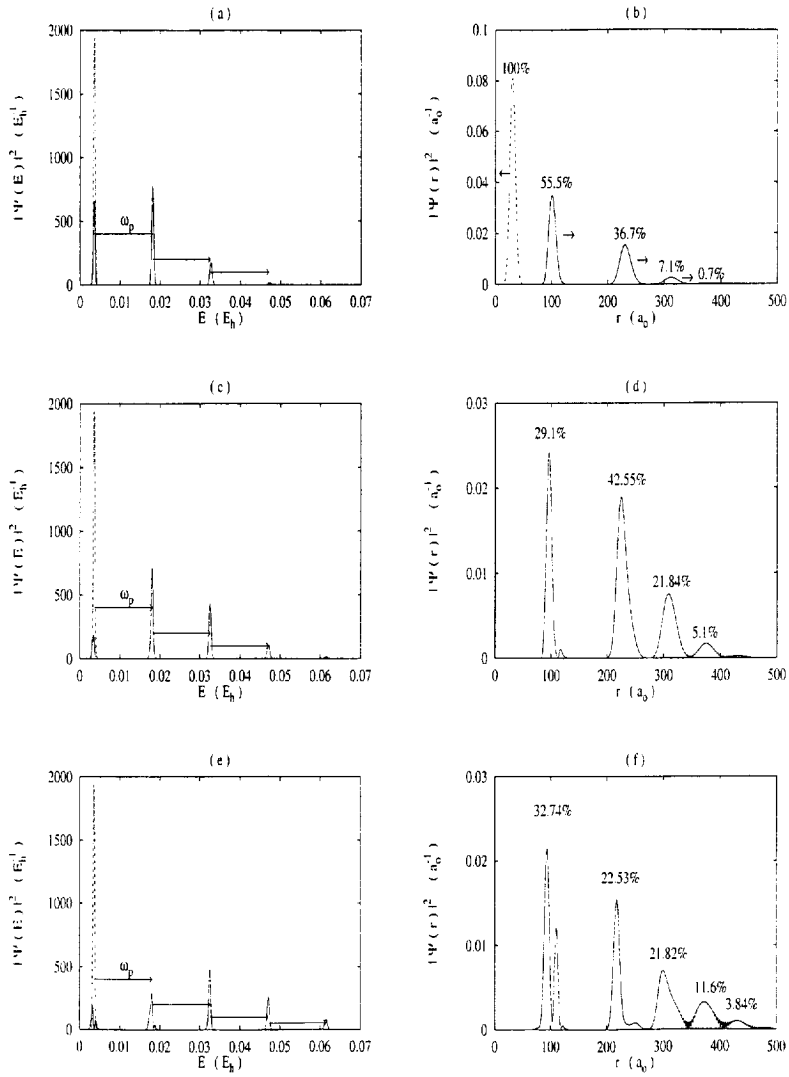

Fig. 5. Effect of laser induced acceleration for constant frequency $\omega_p = 3182.4\ \mathrm{cm}^{-1}$ but for different electric fields $\mathscr{E}_p$ after the end of the laser pulse ($t = 1.5$ ps). The left part shows the probability $|\psi|^2$ in energy representation (in atomic units $E_h = 219450\ \mathrm{cm}^{-1}$), the right half in position space representation (in atomic units $a_0 = 52.92$ pm). In either case, the dot–dashed curve represents the initial state ($t = 0$). (a) and (b) $\mathscr{E}_p = 25.71$ GV/m. (c) and (d) $\mathscr{E}_p = 38.56$ GV/m. (e) and (f) $\mathscr{E}_p = 51.42$ GV/m.

ities in the standing wave pattern at $t = 0.31$ ps, Fig. 3a shows a depletion of the elastically scattered part of the wavefunction for $t = 0.62$ ps while there is another part at much larger internuclear distances which has been accelerated by the laser pulse.

The momentum space representation of Fig. 4 allows an alternative view of the process of laser induced acceleration. The elastic process is characterized by a reversal of the initial momentum of $k_0 = -66.14$ nm^{-1} of the incident Gaussian packet (Fig. 4b). The buildup of the standing wave is accompanied by some broad oscillatory background for both $k < -|k_0|$ and $k > |k_0|$. The effect of the interaction with the infrared laser field (Fig. 4a) is twofold. First, the laser pulse creates some intermediate probability of finding bound states as has been discussed above (see Fig. 2c). The signature of these states can be found in the fast oscillations at momenta $-|k_0| < k < |k_0|$. Second, absorption of one or more photons leads to acceleration of the collision partners which is evident from the formation of four additional peaks in the distribution of momenta at positive values $k > |k_0|$.

Finally, we want to investigate the dependence of acceleration of collision pairs on the intensity of the laser pulse. Fig. 5 shows energy and coordinate space representations of the probability $|\psi(E)|^2$ and $|\psi(r)|^2$, respectively, for various fields $\mathscr{E}_p$. A comparison of initial ($t = 0$, dashed curve) and final ($t = 1.5$ ps, solid curve) energy representations on the left-hand side of Fig. 5 shows that only some fraction of the wavefunction is scattered elastically while the remaining probability is found at higher energies corresponding to the absorption of one or more quanta of the electric field. In the following, we compare the areas under the peaks of the probability distributions which are obtained by numerical integration. Increasing the field from 25.71 GV/m (Fig. 5a,b) to 38.56 GV/m (Fig. 5c,d) reduces the probability of elastical scattering from 55.5% down to 29.1%. At the same time, inelastic scattering starts to dominate, with especially increased probability of multi-photon processes, e.g. the probability of absorbing two photons increases from 7.1% to 21.8%. A further increase of the laser intensity ($\mathscr{E}_p = 51.42$ GV/m) leads to effects which are similar to hole burning in spectroscopy (see Fig. 5e and Fig. 5f). Due to a sharp resonance condition both in frequency and in time (close to the maximum of the laser pulse) there is a dip-like depletion of the elastically scattered and the first accelerated wavepacket.

4. Discussion

This work presents a first study of the photon-induced dynamics of a collision pair interacting with an infrared picosecond laser pulse. There is a competition between non-reactive processes such as elastic and inelastic scattering of collision partners and reactive processes induced by infrared picosecond laser pulses. In the case of inelastic scattering, absorption of one (or more) photons leads to acceleration of the collision partners. In the case of reactive scattering, induced emission of one (or more) photon results in stabilization of the complex leading to (permanent) photoassociation.

An experimental approach to these bimolecular processes would have to address the issue of the timing of the laser pulse relative to the collision event. This could be realized by a pump–probe technique employing two laser pulses. For example, the initial state of Eq. (1) could be prepared by a preceding photodissociation, or the final vibrational dynamics of the molecular photoassociation product could be monitored by an appropriate probe mechanism. The latter possibility has recently been demonstrated both in experiment [18] and in theory [19] for the exciplex formation of mercury.

It is shown that for the example of the O + H collision and for the fields considered here (between 10 and 50 GV/m) there are many different resonance frequencies for continuum → bound transitions due to one-, two-, and three-photon processes. However, for frequencies sufficiently far from one of the continuum → bound resonances, reactive events can be completely excluded. For these cases it is shown that for increasing laser intensity the probability of elastic scattering is lowered while the probability for higher-order processes increases corresponding to higher acceleration of the collision partners. This process exhibits certain analogies with the phenomenon of above threshold dissociation (ATD) in which the peaks of the kinetic energy distribution of the photofragments are separated by the photon energy [4]. It is noted that also coherent control schemes

have been devised to control the process of ATD which in future work could be applied to the processes investigated here. These schemes employ phase effects in coherent superpositions of a laser pulse with one of its harmonics [20,21].

In our example, accelerations of up to 1.6 eV can be achieved by absorption of four photons. Thus, the method of laser induced acceleration as it is suggested here represents an alternative to the method proposed in Ref. [10] where molecules are vibrationally excited in a supersonic expansion which via subsequent vibration–translation energy transfer also leads to acceleration of the particles involved. However, there is a principle limitation of our method with respect to the maximum acceleration that can be gained. First, the laser frequency can only be increased in a limited range because of the decreasing matrix elements of the dipole moment operator for continuum → continuum transitions. Second, the alternative strategy of increasing the laser intensity in order to reach higher acceleration by absorption of more and more photons has also to be limited. Because of the increased density of resonances for higher-order continuum → bound transitions, associative events are competing with continuum → continuum transitions.

Acknowledgements

Financial support by the Deutsche Forschungsgemeinschaft (DFG) through grant Ma 515/14–1 is gratefully acknowledged. Furthermore, we would like to thank J. Manz and G.K. Paramonov for stimulating discussions.

References

[1] M.V. Korolkov, J. Manz, G.K. Paramonov, B. Schmidt, Chem. Phys. Lett. 260 (1996) 604.
[2] M. Kaluža, J.T. Muckerman, P. Gross, H. Rabitz, J. Chem. Phys. 100 (1994) 4211.
[3] M. Kaluža, J.T. Muckerman, J. Chem. Phys. 105 (1996) 535.
[4] M.V. Korolkov, G.K. Paramonov, B. Schmidt, J. Chem. Phys. 105 (1996) 1862.
[5] M.V. Korolkov, J. Manz, G.K. Paramonov, Chem. Phys., in press.
[6] L. Frommhold, Collision-induced absorption in gases (Cambridge Univ. Press, Cambridge, 1993).
[7] A. Borysow, M. Moraldi, J. Chem. Phys. 99 (1993) 8424.
[8] S.Y. Epifanov, A.A. Vigasin, Chem. Phys. Lett. 225 (1994) 537.
[9] H. Pauli, in: Atomic and molecular beam methods, ed. G. Scoles (Oxford Univ. Press, Oxford, 1988).
[10] G.N. Makarov, Chem. Phys. Lett. 237 (1995) 361.
[11] J.S. Wright, D.J. Donaldson, Chem. Phys. 94 (1985) 15.
[12] R. Mecke, Z. Elektrochem. 54 (1950) 38.
[13] R.T. Lawton, M.S. Child, Mol. Phys. 40 (1980) 773.
[14] R. Kosloff, J. Phys. Chem. 92 (1988) 2087.
[15] R. Kosloff, Annu. Rev. Phys. Chem. 45 (1994) 145.
[16] M.D. Feit, J.A. Fleck, Jr, A. Steiger, J. Comput. Phys. 47 (1982) 412.
[17] M.D. Feit, J.A. Fleck, Jr, A. Steiger, J. Chem. Phys. 80 (1984) 2578.
[18] U. Marvet, M. Dantus, Chem. Phys. Lett. 245 (1995) 393.
[19] P. Backhaus, B. Schmidt, Chem. Phys., in press.
[20] E. Charron, A. Giusti-Suzor, F.H. Mies, Phys. Rev. Lett. 71 (1993) 692.
[21] E. Charron, A. Giusti-Suzor, F.H. Mies, J. Chem. Phys. 103 (1995) 7359.